

On the Fragility of AI-Based Channel Decoders under Small Channel Perturbations

Haoyu Lei^{*†}, Mohammad Jalali^{*‡}, Chin Wa Lau[§], Farzan Farnia[¶]

Abstract

Recent advances in deep learning have led to AI-based error correction decoders that report empirical performance improvements over traditional belief-propagation (BP) decoding on AWGN channels. While such gains are promising, a fundamental question remains: where do these improvements come from, and what cost is paid to achieve them? In this work, we study this question through the lens of robustness to distributional shifts at the channel output. We evaluate both input-dependent adversarial perturbations (FGM and projected gradient methods under ℓ_2 constraints) and universal adversarial perturbations that apply a single norm-bounded shift to all received vectors. Our results show that recent AI decoders, including ECCT and CrossMPT, could suffer significant performance degradation under such perturbations, despite superior nominal performance under i.i.d. AWGN. Moreover, adversarial perturbations transfer relatively strongly between AI decoders but weakly to BP-based decoders, and universal perturbations are substantially more harmful than random perturbations of equal norm. These numerical findings suggest a potential robustness cost and higher sensitivity to channel distribution underlying recent AI decoding gains.

1 Introduction

Reliable decoding is a cornerstone of digital communication systems. Shannon’s channel coding theorem [1] establishes that rates up to channel capacity are achievable in principle, but approaching these limits in practice critically depends on the design of efficient and accurate decoding algorithms. Over the past decades, this challenge has been addressed through the development of powerful code families and iterative decoding methods, including turbo decoding [2] and belief-propagation (BP) decoding for LDPC codes [3–5]. In modern wireless systems, decoders must operate under stringent constraints on complexity, latency, energy consumption, numerical precision, and robustness to channel mismatch, making decoder design a central bottleneck in translating information-theoretic limits into practical performance [6, 7].

Motivated by the success of deep learning in other domains, recent years have seen growing interest in applying neural network methods to channel decoding. Early learning-based approaches primarily focused on enhancing traditional decoders, for example by parameterizing belief-propagation updates or unrolling iterative decoding algorithms, as in neural BP [8]. Other works explored model-free neural decoders that learn a direct mapping from channel outputs to codewords, particularly in short blocklength regimes [9]. While these approaches demonstrated promising gains in selected settings, they largely preserved the structure of classical decoding algorithms, and thus did not fundamentally depart from traditional message-passing paradigms.

More recently, transformer-based decoder architectures have been proposed that depart more substantially from classical decoding rules. Notably, the Error Correction Code Transformer (ECCT) [10] introduces a transformer-based decoder with code-structure-aware attention mechanisms and reports considerable

^{*}Equal contribution

[†]Department of Computer Science and Engineering, The Chinese University of Hong Kong, hylei22@cse.cuhk.edu.hk

[‡]Department of Computer Science and Engineering, The Chinese University of Hong Kong

[§]Huawei Technologies Co., Ltd., Theory Lab

[¶]Department of Computer Science and Engineering, The Chinese University of Hong Kong, farnia@cse.cuhk.edu.hk

improvements over prior neural decoders. CrossMPT [11] further integrates masked cross-attention between magnitude and syndrome representations and reports empirical performance gains across several code families, including explicit improvements over conventional BP decoding under the considered settings. These results suggest that modern AI decoders may extract performance gains beyond traditional message-passing algorithms, raising a fundamental question: *what is the source of these gains?*

In this work, we study this question through the lens of robustness to distributional shifts at the channel output. Specifically, we ask whether the nominal performance improvements reported for recent AI decoders could come at the cost of increased sensitivity to small, norm-bounded perturbations applied to the received signal. Such perturbations can be interpreted as worst-case deviations from the target AWGN model and correspond to small shifts in the distribution of channel outputs, which are commonly modeled by Wasserstein-type robustness notions [12]. Understanding decoder behavior under these shifts is essential for assessing the reliability of AI-based decoders beyond standard channel assumptions.

To address this question, we adopt tools from the adversarial robustness literature [13, 14] and evaluate both input-dependent and universal perturbations applied to the received vector. We consider fast gradient methods and multi-step projected gradient attacks constrained to an ℓ_2 norm ball, as well as universal adversarial perturbations that apply the same perturbation to all channel outputs [15]. The attacks are implemented at the AWGN channel output and optimized using gradient-based methods with randomized smoothing [16] to stabilize the optimization in the presence of non-smooth decoder mappings.

Our numerical results show that standard, input-dependent adversarial perturbations can induce significant degradation in the frame error rate of recent transformer-based AI decoders, including ECCT [10] and CrossMPT [11]. We further investigate universal perturbations, which are particularly relevant in practice since they do not depend on individual received vectors and could correspond to persistent interference or hardware-induced distortions. We find that universal adversarial perturbations [15] are significantly more harmful to AI decoders than random perturbations with the same ℓ_2 norm. This observation indicates that the degradation cannot be attributed merely to increased noise power, but rather to structured vulnerabilities in the learned decoding rules.

Finally, we study the transferability of adversarial perturbations across decoders, a phenomenon widely observed in adversarial learning [13]. Perturbations optimized for one transformer-based AI decoder often transfer effectively to another, while exhibiting much weaker transferability to BP-based decoders. Conversely, classical decoders remain comparatively robust to perturbations crafted for AI decoders. Together, these results suggest that recent AI decoding gains may rely on brittle, distribution-specific features, and they quantify a robustness cost that would be less present in traditional message-passing decoding.

2 Related Works

AI and ML decoders. Learning-based decoding has evolved from unrolled belief propagation [17] to end-to-end architectures. Examples include feedback coding in Deepcode [18], Turbo Autoencoders [19], and meta-learning adaptations via MIND [20]. Recently, the transformers ECCT [10], CrossMPT [11] and DiffMPT [21] have utilized attention mechanisms to improve conventional baselines. Further models include diffusion-based iterative refinement [22], multi-code foundation models [23], and one-step consistency models [24].

Robustness of AI decoders. Research indicates that learned receivers are highly sensitive to perturbations. Physical adversarial attacks have been shown to significantly degrade end-to-end autoencoders compared to classical schemes [25]. In wireless security, input-agnostic perturbations have been developed for DNN-based systems [26]. Furthermore, deep receivers demonstrate vulnerability to constrained attacks, such as those limited by power and PAPR [27].

Adversarial and distributional robustness in information theory. Classical work investigates reliable communication under worst-case models, centrally the arbitrarily varying channel (AVC) [28]. Related adversarial settings include oblivious channels [29] and causal adversaries [30]. Recently, capacity has been characterized for adversaries with computationally restricted observations [31]. Parallelly, distributional robustness via Wasserstein ambiguity sets [32] provides a framework to connect norm-bounded perturbations

to distribution shifts.

3 Preliminaries

We consider a binary linear error-correcting code with codebook $\mathcal{C} \subset \{0, 1\}^n$, defined by a generator matrix $G \in \mathbb{F}_2^{k \times n}$ and a parity-check matrix $H \in \mathbb{F}_2^{(n-k) \times n}$ satisfying $GH^\top = 0$ over \mathbb{F}_2 . A message $m \in \{0, 1\}^k$ is encoded as the codeword $x = mG \in \mathcal{C}$ and modulated using Binary Phase-Shift Keying (BPSK), where $0 \mapsto +1$ and $1 \mapsto -1$, yielding the transmitted codeword $x_s \in \{-1, +1\}^n$. The codeword is transmitted over an Additive White Gaussian Noise (AWGN) channel, and the received signal is

$$y = x_s + z, \quad (1)$$

where the noise vector $z \sim \mathcal{N}(0, \sigma^2 I_n)$ is drawn from a Gaussian distribution. The goal of the decoder is to estimate the transmitted codeword \hat{x}_s from observed y .

An important quantity used in decoding is the syndrome, which is computed from a hard-demodulated version of the received signal. Specifically, we define $y_b = \text{bin}(\text{sign}(y))$, where $\text{sign}(y_i) = +1$ if $y_i \geq 0$ and -1 otherwise, and $\text{bin}(\cdot)$ maps $\{-1, +1\}$ to $\{1, 0\}$. The corresponding syndrome is $s(y) = Hy_b^\top \in \mathbb{F}_2^{n-k}$, and an error is detected whenever $s(y) \neq 0$.

Following the preprocessing strategy of [33], the input to the neural decoder is constructed by concatenating the magnitude of the received signal with the syndrome,

$$\phi(y) = [|y|, s(y)], \quad (2)$$

resulting in an input vector of dimension $n + (n - k)$. This representation exposes both reliability information and parity-check violations to the neural decoder and has been shown to reduce overfitting while preserving decoding performance.

4 Robustness of AI Decoders to Input Perturbations

We study the worst-case sensitivity of channel decoders to small perturbations applied at the channel output. Let f denote a decoder (classical or AI-based) mapping a channel observation $y \in \mathbb{R}^n$ to an estimate $\hat{x}_s \in \{-1, 1\}^n$. Let $x^* \in \{-1, 1\}^n$ denote the transmitted codeword, we train the AI decoder by optimizing:

$$\min_{f \in \mathcal{F}} \mathbb{E} \left[\ell(f(y), x^*) \right], \quad (3)$$

where $\ell(\cdot, \cdot)$ denotes the loss function, specifically the Binary Cross Entropy (BCE) as defined in [11, 34].

Sample-wise adversarial objective. Given a perturbation budget $\varepsilon > 0$, we define the sample-wise ℓ_2 -bounded adversarial perturbation as

$$\max_{\delta \in \mathbb{R}^n} \ell(f(y + \delta), x^*) \quad \text{s.t.} \quad \|\delta\|_2 \leq \varepsilon. \quad (4)$$

Directly optimizing (4) can be challenging when f includes hard operations (e.g., sign, binarization, syndrome computation), which may yield non-smooth or unstable gradients. We therefore attack a smoothed surrogate as explained below.

Randomized smoothing of the decoder optimization objective. Fix $\nu > 0$ and let $V \sim \mathcal{N}(0, \nu^2 I_n)$. We define the Gaussian-smoothed loss

$$g(y, \delta) \triangleq \mathbb{E}_{V \sim \mathcal{N}(0, \nu^2 I_n)} \left[\ell(f(y + V + \delta), x^*) \right], \quad (5)$$

and consider the smoothed adversarial objective

$$\max_{\|\delta\|_2 \leq \varepsilon} g(y, \delta). \quad (6)$$

Randomized smoothing yields a stable gradient signal and enables principled gradient-based attacks.

To understand why the randomized smoothing helps, we observe in the following proposition that Gaussian smoothing makes the loss landscape well-behaved in a *dimension-free* way. This is a key technical tool for the universal-perturbation analysis in Section 4.2, where we will both (i) justify gradient-based optimization of universal objectives and (ii) derive a closed-form universal direction (UAP-PCA) from a smoothness surrogate.

Proposition 4.1 (Dimension-free smoothness via Gaussian smoothing). *Assume the loss is bounded: for all $u \in \mathbb{R}^n$,*

$$0 \leq \ell(f(u), x^*) \leq C. \quad (7)$$

Define $\tilde{g}(u) \triangleq \mathbb{E}_{V \sim \mathcal{N}(0, \nu^2 I_n)} [\ell(f(u + V), x^*)]$. Then \tilde{g} has a Lipschitz-continuous gradient with constant

$$\beta \leq \frac{C}{\nu^2} \mathbb{E}[|Z^2 - 1|] < \frac{C}{\nu^2}, \quad Z \sim \mathcal{N}(0, 1), \quad (8)$$

i.e., $\|\nabla \tilde{g}(u) - \nabla \tilde{g}(u')\|_2 \leq \frac{C}{\nu^2} \|u - u'\|_2$ for all u, u' .

Proof. We defer the proof to the Appendix A. \square

4.1 Sample-wise adversarial attacks

We consider two standard first-order attacks on the smoothed objective (6). Both attacks estimate $\nabla_\delta g(y, \delta)$ using Monte Carlo samples $V_1, \dots, V_M \sim \mathcal{N}(0, \nu^2 I_n)$:

$$\nabla_\delta g(y, \delta) \approx \frac{1}{M} \sum_{m=1}^M \nabla_\delta \ell(f(y + \delta + V_m), x^*). \quad (9)$$

PGD Attack Projected Gradient Descent (PGD) [35] performs iterative projected gradient ascent on (6):

$$\delta^{(t+1)} = \Pi_\varepsilon \left(\delta^{(t)} + \eta \nabla_\delta g(y, \delta^{(t)}) \right), \quad t = 0, \dots, T-1, \quad (10)$$

where Π_ε denotes Euclidean projection onto $\{\delta : \|\delta\|_2 \leq \varepsilon\}$. PGD refines δ over multiple steps and typically yields stronger attacks than a single gradient step.

FGM Attack The Fast Gradient Method (FGM) [13] is a single-step attack that linearizes $g(y, \delta)$ at $\delta = 0$ and selects the maximizer of the linear approximation under the ℓ_2 constraint:

$$\delta_{\text{FGM}} = \varepsilon \frac{\nabla_\delta g(y, 0)}{\|\nabla_\delta g(y, 0)\|_2}. \quad (11)$$

FGM is computationally efficient and serves as a baseline for first-order vulnerability.

4.2 Universal adversarial perturbations

Universal adversarial perturbations (UAPs) [36] seek a single perturbation that degrades performance across many channel outputs. Let \mathcal{D} denote the distribution of (Y, X^*) induced by random messages and channel noise. Define the population and empirical universal objectives

$$F(\delta) \triangleq \mathbb{E}_{(Y, X^*) \sim \mathcal{D}} [g(Y, \delta)], \quad \widehat{F}_N(\delta) \triangleq \frac{1}{N} \sum_{i=1}^N g(Y_i, \delta), \quad (12)$$

where $(Y_i, X_i^*)_{i=1}^N$ are i.i.d. samples from \mathcal{D} .

UAP-Grad Our first universal attack, *UAP-Grad*, directly applies projected gradient ascent to the empirical objective $\widehat{F}_N(\delta)$:

$$\delta^{(t+1)} = \Pi_\varepsilon \left(\delta^{(t)} + \eta \cdot \frac{1}{N} \sum_{i=1}^N \nabla_\delta g(Y_i, \delta^{(t)}) \right). \quad (13)$$

UAP-Grad is flexible and powerful but can be computationally demanding due to repeated gradient aggregation across many samples.

UAP-PCA Our second approach, *UAP-PCA*, provides a closed-form universal direction motivated by smoothness. For each sample i , define the smoothed per-sample function

$$\tilde{g}_i(u) \triangleq \mathbb{E}_{V \sim \mathcal{N}(0, \nu^2 I_n)} \left[\ell(f(u + V), X_i^*) \right],$$

and its gradient at the sample input

$$q_i \triangleq \nabla \tilde{g}_i(Y_i) \in \mathbb{R}^n. \quad (14)$$

UAP-PCA computes the universal direction from the empirical second-moment matrix

$$\widehat{\Sigma}_q \triangleq \frac{1}{N} \sum_{i=1}^N q_i q_i^\top. \quad (15)$$

Note that Proposition 4.1 implies β -smoothness for Gaussian-smoothed losses under boundedness. For UAP-PCA, we further exploit smoothness to build a quadratic lower bound in a fixed direction, then optimize that surrogate exactly. This yields an *exact PCA* characterization.

Proposition 4.2. *Assume every \tilde{g}_i is β -smooth. For a unit direction $\delta \in \mathbb{R}^n$ with $\|\delta\|_2 = 1$, smoothness implies that for all $\alpha \in \mathbb{R}$,*

$$\tilde{g}_i(Y_i + \alpha \delta) \geq \tilde{g}_i(Y_i) + \alpha \delta^\top q_i - \frac{\beta}{2} \alpha^2. \quad (16)$$

Consider the surrogate maximization problem

$$\max_{\delta \in \mathbb{R}^n: \|\delta\|_2=1} \frac{1}{N} \sum_{i=1}^N \max_{\alpha \in \mathbb{R}} \left(\alpha \delta^\top q_i - \frac{\beta}{2} \alpha^2 \right). \quad (17)$$

Then any maximizer δ^* of (17) is a top eigenvector of $\widehat{\Sigma}_q$ defined in (15).

Proof. We defer the proof to the Appendix A. □

Finite-sample guarantees for UAP evaluation and UAP-PCA

We next state a concentration theorem that (i) quantifies how many samples suffice to estimate the universal objective $\widehat{F}_N(\delta)$ for a fixed δ , and (ii) guarantees stability of the empirical top principal component \hat{u}_1 of $\widehat{\Sigma}_q$. *Assumptions.* We assume (a) bounded loss $0 \leq \ell(\cdot) \leq C$, (b) bounded gradients $\|q_i\|_2 \leq L$ almost surely, and (c) an eigengap $\Delta \triangleq \lambda_1(\Sigma_q) - \lambda_2(\Sigma_q) > 0$, where $\Sigma_q \triangleq \mathbb{E}[qq^\top]$ and q denotes a generic copy of q_i .

Theorem 4.3 (Concentration for UAP objective and UAP-PCA). *Fix any $\eta \in (0, 1)$. Given assumptions (a), (b), (c), then with probability at least $1 - \eta$, the following hold:*

$$|\widehat{F}_N(\delta) - F(\delta)| \leq C \sqrt{\frac{\log(4/\eta)}{2N}} \quad \text{for any fixed } \delta, \quad (18)$$

$$\|\widehat{\Sigma}_q - \Sigma_q\|_{\text{op}} \leq 4\sqrt{2} L^2 \sqrt{\frac{\log(4n/\eta)}{N}}, \quad (19)$$

$$\sin \angle(\hat{u}_1, u_1) \leq \frac{4\sqrt{2} L^2}{\Delta} \sqrt{\frac{\log(4n/\eta)}{N}}, \quad (20)$$

where u_1 is the top eigenvector of Σ_q , \hat{u}_1 is the top eigenvector of $\widehat{\Sigma}_q$ (with sign chosen to maximize $|\langle \hat{u}_1, u_1 \rangle|$), and $\angle(\cdot, \cdot)$ denotes the principal angle between one-dimensional subspaces.

Proof. We defer the proof to the Appendix A. \square

5 Numerical Results

5.1 Experimental Setup

Datasets. We evaluate the adversarial attack on standard error correction codes, specifically focusing on Polar and LDPC codes. Our evaluation spans various code configurations, including different code lengths (n) and code rates ($R = k/n$). Furthermore, we test across a range of Signal-to-Noise Ratios (SNRs), specifically targeting E_b/N_0 from 4 to 6 dB. We evaluate results on 10^6 test samples for each code type.

Evaluation Metrics. Following existing works [34, 37], we assess decoding performance using the standard metric: Frame Error Rate (FER), quantifying the fraction of codewords containing at least one bit error.

Baselines. We evaluate the adversarial attacks against a comprehensive set of decoding algorithms, categorized into: 1) Traditional Decoders: Min-Sum (MS) [5, 38] and Sum-Product (SP) [3, 39] with maximum number of iterations equals 10. 2) Neural Decoders: State-of-the-art deep learning-based methods, specifically ECCT [34] and CrossMPT [37]. For the neural decoders (ECCT, CrossMPT), we follow the settings specified in their publications to ensure fair comparison. Both models are implemented with a depth of $N = 6$ layers and a hidden dimension of $d = 128$.

Adversarial Attack Methods. We evaluate the decoders against both sample-level and universal adversarial attacks. For sample-level attacks, which target individual codewords, we apply Fast Gradient Method (FGM) [40] and Projected Gradient Descent (PGD) [35]. For universal attacks, which seek a single perturbation across the dataset, we choose Universal Adversarial Perturbation (UAP) [36] and PCA-based Universal Adversarial Direction (UAP-PCA) [41]. For all attack methods, we constrain the perturbation energy using a relative L_2 -norm bound: $\|\delta\|_2 \leq \alpha \|y\|_2$. Additionally, we report results under random noise with the same energy constraint to demonstrate the impact of adversarial attack.

5.2 Performance Drop after Adversarial Attack

In our experiments, we evaluate the robustness of two baseline AI decoders, CrossMPT and ECCT, against various attack methods, including FGM, PGD, UAP, and UAP-PCA. We compare the performance in terms of the inverse Frame Error Rate (**1/FER**) before and after applying attacks. The same energy constraint of $\alpha = 0.001$ is applied across all attack methods. We conduct experiments on different Polar and LDPC codes with E_b/N_0 ranging from 4 to 6 dB. As shown in Table 1, although the well-trained AI decoders initially exhibit superior decoding performance, adversarial perturbations with merely $\frac{1}{1000}$ of the signal energy cause a significant degradation. While the decoders remain relatively robust to random noise, we observe a sharp decline in performance under adversarial attacks, especially at high SNRs. For decoding LDPC(49,24) at 6dB, the (**1/FER**) decreases from 5.0×10^4 to 2.6×10^1 under the PGD attack, indicating a performance drop over 1000 times. This reveals the robustness cost inherent in AI decoders under adversarial attacks.

Table 1: Decoding Performance comparison using the **FER-Inverse (1/FER)** under different attack methods.

Type	Method	SNR	ECCT				CrossMPT			
			Polar		LDPC		Polar		LDPC	
			(64,48)↑	(128,64)↑	(49,24)↑	(121,60)↑	(64,48)↑	(128,64)↑	(49,24)↑	(121,60)↑
w/o attack	Clean	4	2.1×10^1	8.5×10^0	3.7×10^1	8.6×10^0	3.4×10^1	2.5×10^1	8.9×10^1	2.1×10^1
		5	1.6×10^2	7.4×10^1	3.5×10^2	1.4×10^2	2.6×10^2	2.4×10^2	1.5×10^3	6.1×10^2
		6	2.2×10^3	1.4×10^3	9.1×10^3	1.1×10^4	4.8×10^3	1.0×10^4	5.0×10^4	1.7×10^4
	Random	4	2.0×10^1	8.1×10^0	3.5×10^1	8.2×10^0	3.3×10^1	3.0×10^1	7.7×10^1	1.9×10^1
		5	1.3×10^2	5.9×10^1	2.4×10^2	9.3×10^1	2.2×10^2	1.7×10^2	1.2×10^3	2.7×10^2
		6	1.7×10^3	6.1×10^2	2.0×10^3	3.6×10^3	2.8×10^3	4.5×10^3	9.8×10^3	3.8×10^3
	UAP	4	1.7×10^1	5.4×10^0	2.8×10^1	5.1×10^0	2.8×10^1	1.9×10^1	4.0×10^1	1.6×10^1
		5	5.3×10^1	3.4×10^1	1.1×10^2	3.2×10^1	1.0×10^2	7.3×10^1	2.0×10^2	5.5×10^1
		6	3.6×10^2	9.8×10^1	2.7×10^2	2.0×10^2	5.7×10^2	5.7×10^2	6.4×10^2	5.1×10^2
Universal	UAP-PCA	4	1.5×10^1	5.0×10^0	2.4×10^1	4.7×10^0	2.4×10^1	1.3×10^1	3.5×10^1	1.4×10^1
		5	4.5×10^1	2.0×10^1	9.8×10^1	2.1×10^1	6.9×10^1	5.6×10^1	1.6×10^2	4.5×10^1
		6	1.5×10^2	5.8×10^1	1.6×10^1	1.1×10^2	2.4×10^2	1.9×10^2	3.4×10^2	1.9×10^2
	FGM	4	1.4×10^1	4.9×10^0	2.0×10^1	4.1×10^0	2.2×10^1	8.4×10^0	2.9×10^1	1.3×10^1
		5	3.2×10^1	1.4×10^1	5.5×10^1	1.5×10^1	3.8×10^1	4.7×10^1	1.2×10^2	3.1×10^1
		6	7.1×10^1	2.8×10^1	9.3×10^1	6.3×10^1	7.5×10^1	1.2×10^2	1.7×10^2	1.1×10^2
	PGD	4	7.8×10^0	3.0×10^0	6.0×10^0	3.3×10^0	9.0×10^0	3.5×10^0	1.0×10^1	6.8×10^0
		5	1.8×10^1	5.4×10^0	9.3×10^0	8.3×10^0	1.7×10^1	6.9×10^0	1.5×10^1	1.8×10^1
		6	3.3×10^1	8.3×10^0	1.5×10^1	1.7×10^1	3.2×10^1	1.9×10^1	2.6×10^1	3.0×10^1
Sample-level										

5.3 Ablation Study: Change of Energy Constraint

This ablation study investigates how perturbation strength affects performance by varying the energy constraint α ($\|\delta\|_2 \leq \alpha \|y\|_2$) between 10^{-4} and 10^{-1} . Evaluating ECCT on Polar(128,64) across different SNRs, Figure 1 illustrates that degradation becomes progressively more severe with larger energy constraints, an effect that is especially pronounced at high SNRs. Detailed Results for LDPC codes refer to Appendix D.1.

5.4 Transferability of Adversarial Perturbation

We further evaluate the transferability of adversarial perturbations and assess the robustness of traditional decoders. We generate optimal UAP and PGD perturbations based on the ECCT model for the LDPC(121,60) code, under an energy constraint of $\alpha = 0.001$. The decoding performance, measured by **1/FER**, is tested across AI decoders (ECCT, CrossMPT) and traditional decoders (Min-Sum, Sum-Product) under four conditions: clean, random noise, and the transferred UAP and PGD perturbations. As shown in Table 2, while AI decoders achieve superior performance on clean data, they exhibit significant fragility under attack. Notably, the perturbations crafted for ECCT successfully transfer to CrossMPT, causing a drastic performance degradation (e.g., from 1.7×10^4 to 5.5×10^1 at 6 dB under PGD). In contrast, traditional decoders demonstrate robustness, maintaining consistent performance levels even with adversarial distribution shifts. Additional Results, including transferability to diffusion-based DDECC [22] on both LDPC and Polar codes, refer to Appendix D.2.

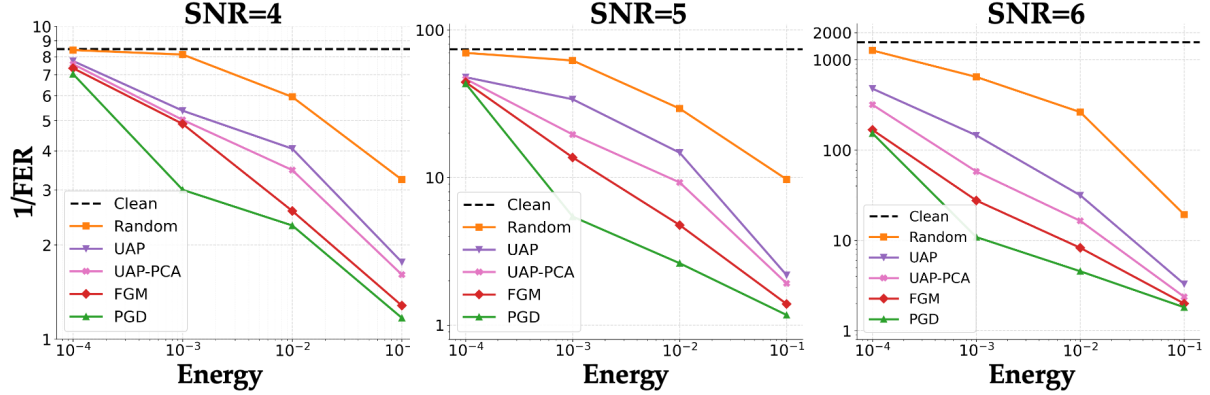


Figure 1: Comparison of **FER-Inverse (1/FER)** under various energy constraints for ECCT on Polar(128,64).

Table 2: Evaluation of attack transferability measured by **FER-Inverse (1/FER)** across decoders on LDPC(121,60).

Type	Decoder	Attack	4 dB	5 dB	6 dB
AI Decoder	ECCT	Clean	8.6×10^0	1.4×10^2	1.1×10^4
		Random	8.2×10^0	9.3×10^1	3.6×10^3
		UAP	5.1×10^0	3.2×10^1	8.0×10^2
		PGD	3.3×10^0	8.3×10^0	1.7×10^1
AI Decoder	CrossMPT	Clean	2.1×10^1	6.1×10^2	1.7×10^4
		Random	1.9×10^1	2.7×10^2	3.8×10^3
		UAP	1.7×10^1	6.7×10^1	8.8×10^2
		PGD	9.2×10^0	3.2×10^1	5.5×10^1
Traditional Decoder	Min-sum	Clean	5.4×10^0	5.1×10^1	2.0×10^3
		Random	5.4×10^0	5.1×10^1	1.9×10^3
		UAP	5.3×10^0	5.0×10^1	1.7×10^3
		PGD	5.0×10^0	4.3×10^1	1.3×10^3
Traditional Decoder	Sum-product	Clean	1.6×10^1	4.9×10^2	1.5×10^4
		Random	1.6×10^1	4.8×10^2	1.4×10^4
		UAP	1.5×10^1	4.1×10^2	1.1×10^4
		PGD	1.3×10^1	3.3×10^2	1.0×10^4

6 Conclusion and Limitations

This work indicates that although recent AI-based decoders can outperform traditional baselines under nominal AWGN conditions, their performance may be more sensitive to small, worst-case input perturbations crafted for these models. Across both input-dependent and universal attacks, gains under the standard channel model do not necessarily persist under adversarial perturbations, while BP decoders appear less affected by AI-decoder-targeted perturbations. Future work should explore robustness-aware designs and broader channel models.

References

- [1] Claude E. Shannon. A mathematical theory of communication. *The Bell System Technical Journal*, 27(3):379–423, 1948.
- [2] Claude Berrou, Alain Glavieux, and Punya Thitimajshima. Near shannon limit error-correcting coding and decoding: Turbo-codes. In *Proceedings of IEEE International Conference on Communications (ICC)*, pages 1064–1070, 1993.
- [3] Robert G. Gallager. Low-density parity-check codes. *IRE Transactions on Information Theory*, 8(1):21–28, 1962.
- [4] R. Michael Tanner. A recursive approach to low complexity codes. *IEEE Transactions on Information Theory*, 27(5):533–547, 1981.
- [5] Tom Richardson and Rüdiger Urbanke. *Modern Coding Theory*. Cambridge University Press, 2008.
- [6] 3GPP TS 38.212: NR; multiplexing and channel coding (release 15). Technical Report TS 138 212 V15.2.0, 3rd Generation Partnership Project (3GPP) / ETSI, July 2018.
- [7] Zeynep B. Kaykac Egilmez, Luping Xiang, Robert G. Maunder, and Lajos Hanzo. The development, operation and performance of the 5g polar codes. *IEEE Communications Surveys & Tutorials*, 2020.
- [8] Eliya Nachmani, Yair Be’ery, and David Burshtein. Learning to decode linear codes using deep learning. In *54th Annual Allerton Conference on Communication, Control, and Computing (Allerton)*, pages 341–346. IEEE, 2016.
- [9] Tobias Gruber, Sebastian Cammerer, Jakob Hoydis, and Stephan ten Brink. On deep learning-based channel decoding. *arXiv preprint arXiv:1701.07738*, 2017.
- [10] Yoni Choukroun and Lior Wolf. Error correction code transformer. In *Advances in Neural Information Processing Systems*, 2022.
- [11] Seong-Joon Park, Hee-Youl Kwak, Sang-Hyo Kim, Yongjune Kim, and Jong-Seon No. Crossmpt: Cross-attention message-passing transformer for error correcting codes. In *International Conference on Learning Representations (ICLR)*, 2025.
- [12] Peyman Mohajerin Esfahani and Daniel Kuhn. Data-driven distributionally robust optimization using the Wasserstein metric: Performance guarantees and tractable reformulations. *Mathematical Programming*, 171(1-2):115–166, 2018.
- [13] Ian J. Goodfellow, Jonathon Shlens, and Christian Szegedy. Explaining and harnessing adversarial examples. *International Conference on Learning Representations (ICLR)*, 2015.
- [14] Aleksander Madry, Aleksandar Makelov, Ludwig Schmidt, Dimitris Tsipras, and Adrian Vladu. Towards deep learning models resistant to adversarial attacks. In *International Conference on Learning Representations (ICLR)*, 2018.
- [15] Seyed-Mohsen Moosavi-Dezfooli, Alhussein Fawzi, Omar Fawzi, and Pascal Frossard. Universal adversarial perturbations. In *Proceedings of the IEEE Conference on Computer Vision and Pattern Recognition (CVPR)*, pages 1765–1773, 2017.
- [16] Jeremy M. Cohen, Elan Rosenfeld, and J. Zico Kolter. Certified adversarial robustness via randomized smoothing. In *Proceedings of the 36th International Conference on Machine Learning (ICML)*, volume 97 of *Proceedings of Machine Learning Research*, pages 1310–1320, 2019.

[17] Eliya Nachmani, Yair Be’ery, and David Burshtein. Learning to decode linear codes using deep learning. In *54th Annual Allerton Conference on Communication, Control, and Computing (Allerton)*, pages 341–346. IEEE, 2016.

[18] Hyeji Kim, Yihan Jiang, Sreeram Kannan, Sewoong Oh, and Pramod Viswanath. Deepcode: Feedback codes via deep learning. In *Advances in Neural Information Processing Systems (NeurIPS)*, volume 31, 2018.

[19] Yihan Jiang, Hyeji Kim, Himanshu Asnani, Sreeram Kannan, Sewoong Oh, and Pramod Viswanath. Turbo autoencoder: Deep learning based channel codes for point-to-point communication channels. In *Advances in Neural Information Processing Systems (NeurIPS)*, volume 32, 2019.

[20] Yihan Jiang, Hyeji Kim, Himanshu Asnani, and Sreeram Kannan. Mind: Model independent neural decoder. *arXiv preprint arXiv:1903.02268*, 2019.

[21] Chin Wa Ken Lau, Xiang Shi, Ziyan Zheng, Haiwen Cao, and Nian Guo. Interplay between belief propagation and transformer: Differential-attention message passing transformer. In *2025 IEEE International Symposium on Information Theory (ISIT)*, pages 1–6. IEEE, 2025.

[22] Yoni Choukroun and Lior Wolf. Denoising diffusion error correction codes. In *International Conference on Learning Representations (ICLR)*, 2023.

[23] Yoni Choukroun and Lior Wolf. A foundation model for error correction codes. In *International Conference on Learning Representations (ICLR)*, 2024.

[24] Haoyu Lei, Chin Wa Lau, Kaiwen Zhou, Nian Guo, and Farzan Farnia. Consistency flow model achieves one-step denoising error correction codes. *arXiv preprint arXiv:2512.01389*, 2025.

[25] Meysam Sadeghi and Erik G. Larsson. Physical adversarial attacks against end-to-end autoencoder communication systems. *IEEE Communications Letters*, 23(11):1985–1988, 2019.

[26] Alireza Bahramali, Milad Nasr, Amir Houmansadr, Dennis Goeckel, and Don Towsley. Robust adversarial attacks against DNN-based wireless communication systems. In *Proceedings of the 2021 ACM SIGSAC Conference on Computer and Communications Security (CCS)*, pages 126–140, 2021.

[27] Jinyin Chen, Jie Ge, Shilian Zheng, Linhui Ye, Haibin Zheng, Weiguo Shen, Keqiang Yue, and Xiaoniu Yang. AIR: Threats of adversarial attacks on deep learning-based information recovery. *arXiv preprint arXiv:2309.16706*, 2023.

[28] Imre Csiszár and Prakash Narayan. The capacity of the arbitrarily varying channel revisited: Positivity, constraints. *IEEE Transactions on Information Theory*, 34(2):181–193, 1988.

[29] Michael Langberg. Oblivious communication channels and their capacity. *IEEE Transactions on Information Theory*, 54(1):424–429, 2008.

[30] Yihan Zhang, Sidharth Jaggi, Michael Langberg, and Anand D. Sarwate. The capacity of causal adversarial channels. In *2022 IEEE International Symposium on Information Theory (ISIT)*, pages 766–771, 2022.

[31] Eric Ruzomberka, Chih-Chun Wang, and David J. Love. Channel capacity for adversaries with computationally bounded observations. *IEEE Transactions on Information Theory*, 69(11):6850–6881, 2023.

[32] Peyman Mohajerin Esfahani and Daniel Kuhn. Data-driven distributionally robust optimization using the Wasserstein metric: Performance guarantees and tractable reformulations. *Mathematical Programming*, 171(1-2):115–166, 2018.

- [33] Amir Bennatan, Yoni Choukroun, and Pavel Kisilev. Deep learning for decoding of linear codes-a syndrome-based approach. In *2018 IEEE International Symposium on Information Theory (ISIT)*, pages 1595–1599. IEEE, 2018.
- [34] Yoni Choukroun and Lior Wolf. Error correction code transformer. *Advances in Neural Information Processing Systems*, 35:38695–38705, 2022.
- [35] Aleksander Madry, Aleksandar Makelov, Ludwig Schmidt, Dimitris Tsipras, and Adrian Vladu. Towards deep learning models resistant to adversarial attacks. *arXiv preprint arXiv:1706.06083*, 2017.
- [36] Seyed-Mohsen Moosavi-Dezfooli, Alhussein Fawzi, Omar Fawzi, and Pascal Frossard. Universal adversarial perturbations. In *Proceedings of the IEEE conference on computer vision and pattern recognition*, pages 1765–1773, 2017.
- [37] Seong-Joon Park, Hee-Youl Kwak, Sang-Hyo Kim, Yongjune Kim, and Jong-Seon No. Crossmpt: Cross-attention message-passing transformer for error correcting codes. In *The Thirteenth International Conference on Learning Representations*, 2025.
- [38] Marc PC Fossorier, Miodrag Mihaljevic, and Hideki Imai. Reduced complexity iterative decoding of low-density parity check codes based on belief propagation. *IEEE Transactions on communications*, 47(5):673–680, 1999.
- [39] F.R. Kschischang, B.J. Frey, and H.-A. Loeliger. Factor graphs and the sum-product algorithm. *IEEE Transactions on Information Theory*, 47(2):498–519, 2001.
- [40] Ian J Goodfellow, Jonathon Shlens, and Christian Szegedy. Explaining and harnessing adversarial examples. *arXiv preprint arXiv:1412.6572*, 2014.
- [41] Ching Lam Choi and Farzan Farnia. Universal adversarial directions. *arXiv preprint arXiv:2210.15997*, 2022.
- [42] Yoni Choukroun and Lior Wolf. Denoising diffusion error correction codes. In *The Eleventh International Conference on Learning Representations*, 2023.
- [43] Erdal Arikan. Channel polarization: A method for constructing capacity-achieving codes for symmetric binary-input memoryless channels. *IEEE Transactions on information Theory*, 55(7):3051–3073, 2009.

Appendix A Proofs

A.1 Proof of Proposition 4.1

To prove Proposition 4.1, let $V \sim \mathcal{N}(0, \nu^2 I_n)$ and define

$$\tilde{g}(u) \triangleq \mathbb{E}[\ell(f(u + V), x^*)].$$

The application of Stein's lemma shows that

$$\nabla \tilde{g}(u) = \frac{1}{\nu^2} \mathbb{E}[\ell(f(u + V), x^*) V]. \quad (21)$$

Considering the second-order differentiation and applying the second-order Stein identity will further yield:

$$\nabla^2 \tilde{g}(u) = \frac{1}{\nu^4} \mathbb{E}[\ell(f(u + V), x^*) (VV^\top - \nu^2 I_n)]. \quad (22)$$

Fix any unit vector $a \in \mathbb{R}^n$ with $\|a\|_2 = 1$. Taking the quadratic form of (22),

$$a^\top \nabla^2 \tilde{g}(u) a = \frac{1}{\nu^4} \mathbb{E}[\ell(f(u + V), x^*) ((a^\top V)^2 - \nu^2)]. \quad (23)$$

By (7), $0 \leq \ell \leq C$, hence

$$|a^\top \nabla^2 \tilde{g}(u) a| \leq \frac{C}{\nu^4} \mathbb{E}[(a^\top V)^2 - \nu^2]. \quad (24)$$

Since $a^\top V \sim \mathcal{N}(0, \nu^2)$, we can write $a^\top V = \nu Z$ with $Z \sim \mathcal{N}(0, 1)$. Substituting into (24) yields

$$|a^\top \nabla^2 \tilde{g}(u) a| \leq \frac{C}{\nu^4} \nu^2 \mathbb{E}[|Z^2 - 1|] = \frac{C}{\nu^2} \mathbb{E}[|Z^2 - 1|]. \quad (25)$$

Using the identity for symmetric matrices,

$$\|\nabla^2 \tilde{g}(u)\|_{\text{op}} = \sup_{\|a\|_2=1} |a^\top \nabla^2 \tilde{g}(u) a|,$$

we obtain from (25) that

$$\|\nabla^2 \tilde{g}(u)\|_{\text{op}} \leq \frac{C}{\nu^2} \mathbb{E}[|Z^2 - 1|].$$

A uniform operator-norm bound on the Hessian implies that $\nabla \tilde{g}$ is Lipschitz with constant β given by the same bound, proving (8). Finally, $\mathbb{E}[|Z^2 - 1|] < 1$ (numerically ≈ 0.968), which yields the strict inequality in (8). \blacksquare

A.2 Proof of Proposition 4.2

To prove Proposition 4.2, consider and fix any unit vector δ with $\|\delta\|_2 = 1$. For every index i , define

$$\psi_i(\alpha) \triangleq \alpha^\top \delta^\top q_i - \frac{\beta}{2} \alpha^2.$$

The inner maximization in (17) equals $\max_{\alpha \in \mathbb{R}} \psi_i(\alpha)$. Since ψ_i is a concave quadratic, it has a unique maximizer given by the first-order necessary condition (FONC):

$$\psi'_i(\alpha_i^*) = \delta^\top q_i - \beta \alpha_i^* = 0 \implies \alpha_i^* = \frac{\delta^\top q_i}{\beta}.$$

Substituting α_i^* ,

$$\max_{\alpha \in \mathbb{R}} \psi_i(\alpha) = \psi_i(\alpha_i^*) = \frac{(\delta^\top q_i)^2}{2\beta}.$$

Therefore, the objective in (17) is proportional to

$$\max_{\|\delta\|_2=1} \frac{1}{N} \sum_{i=1}^N (\delta^\top q_i)^2 = \max_{\|\delta\|_2=1} \delta^\top \left(\frac{1}{N} \sum_{i=1}^N q_i q_i^\top \right) \delta = \max_{\|\delta\|_2=1} \delta^\top \widehat{\Sigma}_q \delta.$$

The maximizers of the Rayleigh quotient $\delta^\top \widehat{\Sigma}_q \delta$ over $\|\delta\|_2 = 1$ are precisely the top eigenvectors of $\widehat{\Sigma}_q$. \blacksquare

A.3 Proof of Theorem 4.3

To show the theorem, here we prove (18)–(20) and then apply a union bound.

A.3.1 Proof of the objective concentration in (18)

Fix any perturbation δ . By the bounded loss assumption $0 \leq \ell(\cdot) \leq C$, we have for all y ,

$$0 \leq g(y, \delta) = \mathbb{E}_V [\ell(f(y + V + \delta), x^*)] \leq C.$$

Hence $Z_i \triangleq g(Y_i, \delta)$ are i.i.d. and lie in $[0, C]$ almost surely. Hoeffding's inequality implies

$$\Pr\left(\left|\frac{1}{N} \sum_{i=1}^N Z_i - \mathbb{E}[Z_1]\right| \geq t\right) \leq 2 \exp\left(-\frac{2Nt^2}{C^2}\right).$$

Since $\frac{1}{N} \sum_{i=1}^N Z_i = \widehat{F}_N(\delta)$ and $\mathbb{E}[Z_1] = F(\delta)$,

$$\Pr\left(\left|\widehat{F}_N(\delta) - F(\delta)\right| \geq t\right) \leq 2 \exp\left(-\frac{2Nt^2}{C^2}\right).$$

Setting the right-hand side to $\eta/2$ yields $t = C \sqrt{\log(4/\eta)/(2N)}$, proving (18) with probability at least $1 - \eta/2$.

A.3.2 Matrix concentration: proof of (19)

Define $\Sigma_q = \mathbb{E}[qq^\top]$ and $\widehat{\Sigma}_q = \frac{1}{N} \sum_{i=1}^N q_i q_i^\top$, and let

$$X_i \triangleq q_i q_i^\top - \Sigma_q.$$

Then $\mathbb{E}[X_i] = 0$ and $\widehat{\Sigma}_q - \Sigma_q = \frac{1}{N} \sum_{i=1}^N X_i$. By $\|q_i\|_2 \leq L$,

$$\|q_i q_i^\top\|_{\text{op}} = \|q_i\|_2^2 \leq L^2, \quad \|\Sigma_q\|_{\text{op}} = \|\mathbb{E}[qq^\top]\|_{\text{op}} \leq \mathbb{E}\|qq^\top\|_{\text{op}} = \mathbb{E}\|q\|_2^2 \leq L^2,$$

and thus $\|X_i\|_{\text{op}} \leq 2L^2$ almost surely.

Let $S \triangleq \sum_{i=1}^N X_i$. A standard matrix Hoeffding inequality for independent, mean-zero, self-adjoint matrices with $\|X_i\|_{\text{op}} \leq R$ gives

$$\Pr(\|S\|_{\text{op}} \geq t) \leq 2n \exp\left(-\frac{t^2}{8 \sum_{i=1}^N R^2}\right) = 2n \exp\left(-\frac{t^2}{8NR^2}\right).$$

With $R = 2L^2$ and $t = N\varepsilon$,

$$\Pr\left(\|\widehat{\Sigma}_q - \Sigma_q\|_{\text{op}} \geq \varepsilon\right) = \Pr\left(\|S\|_{\text{op}} \geq N\varepsilon\right) \leq 2n \exp\left(-\frac{N\varepsilon^2}{32L^4}\right).$$

Setting the right-hand side to $\eta/2$ yields

$$\varepsilon = 4\sqrt{2}L^2\sqrt{\frac{\log(4n/\eta)}{N}},$$

which proves (19) with probability at least $1 - \eta/2$.

A.3.3 Principal component concentration: proof of (20)

Let $E \triangleq \widehat{\Sigma}_q - \Sigma_q$ and $\Delta = \lambda_1(\Sigma_q) - \lambda_2(\Sigma_q) > 0$. The Davis–Kahan $\sin \Theta$ theorem (for the top eigenvector) gives

$$\sin \angle(\hat{u}_1, u_1) \leq \frac{\|E\|_{\text{op}}}{\Delta} = \frac{\|\widehat{\Sigma}_q - \Sigma_q\|_{\text{op}}}{\Delta}.$$

Combining with (19) yields (20).

A.3.4 Union bound

The events for (18) and (19) each hold with probability at least $1 - \eta/2$. By a union bound, they hold simultaneously with probability at least $1 - \eta$, which implies (20) as well. \blacksquare

Appendix B Detailed Experimental Setup

In this section, we provide a detailed description of the data generation process, the training details for neural decoders, the hyperparameter configurations for adversarial attacks.

B.1 Data Generation and Code Construction

Channel Model. We simulate the transmission over an Additive White Gaussian Noise (AWGN) channel using Binary Phase Shift Keying (BPSK) modulation. Let $\mathbf{c} \in \{0, 1\}^n$ denote the codeword. The modulated signal is given by $\mathbf{x} = 1 - 2\mathbf{c}$, where $\mathbf{x} \in \{+1, -1\}^n$. The received signal \mathbf{y} is defined as:

$$\mathbf{y} = \mathbf{x} + \mathbf{z}, \quad \mathbf{z} \sim \mathcal{N}(0, \sigma^2 \mathbf{I}_n), \tag{26}$$

where the noise variance σ^2 is determined by the Signal-to-Noise Ratio (SNR) via $\sigma^2 = (2R \cdot 10^{\text{SNR}/10})^{-1}$, with code rate $R = k/n$.

B.2 Training Details for Neural Decoders

To ensure a fair comparison, the neural decoders (ECCT [10] and CrossMPT [37]) are trained from scratch using the same configuration. For each code configuration (n, k) , we generate the training set following the settings in ECCT and CrossMPT. The training samples are generated with SNRs uniformly sampled from the range [2 dB, 8 dB].

Appendix C Adversarial Attack Settings

In this study, we evaluate the robustness of decoders against five distinct attack strategies. All attacks are constrained under the L_2 -norm and the given energy constraint α , where the perturbation δ must satisfy $\|\delta\|_2 \leq \alpha\|y\|_2$.

Random Noise Baseline. To distinguish adversarial attack methods from general sensitivity to channel noise, we choose a random noise baseline. This perturbation is generated by sampling a vector from a standard normal distribution $\mathcal{N}(0, I)$ and normalizing it to a given energy constraint $\|\delta\|_2 \leq \alpha\|y\|_2$.

Fast Gradient Method (FGM). FGM [40] serves as a single-step attack that linearizes the loss function to generate adversarial examples. We implement the L_2 -normalized version, where the perturbation is computed by taking the gradient of the loss with respect to the input, normalizing it to a unit vector, and scaling it to the energy constraint.

Projected Gradient Descent (PGD). PGD [35] seeks to find the optimal perturbation within the ϵ -ball. We set the attack with $T = 20$ iterations. We initialize with a random perturbation and use a step size of $\alpha = 1.2 \times (\epsilon/20)$, projecting the adversarial perturbation back onto the ϵ -ball satisfying energy constraint.

Universal Adversarial Perturbation (UAP). UAP [36] aims to find an input-agnostic perturbation vector that degrades performance across the entire dataset. We optimize this universal vector using Stochastic Gradient Descent Accumulation (SGDA) over a training set of 50 batches. The optimization uses a learning rate of $\eta = 0.05$, with the perturbation clipped at each step to ensure it satisfies the energy constraint.

PCA-based UAP (UAP-PCA). UAP-PCA [41] applies Principal Component Analysis (PCA) to select the universal perturbation. We collect gradients from 50 batches of samples and apply PCA. The final attack vector is constructed by aligning the perturbation with the Top-1 principal component of the gradient matrix, scaled to the energy constraint.

Appendix D Additional Experimental Results

D.1 Ablation Study: Change of Energy Constraint

In this section, we present additional results on the impact of varying perturbation energy constraints on LDPC(121,60) codes, as shown in Figure 2. We observe a consistent trend: as the energy constraint increases, the performance degradation becomes more severe. Furthermore, adversarial attacks consistently induce significantly higher error rates compared to the random noise baseline.

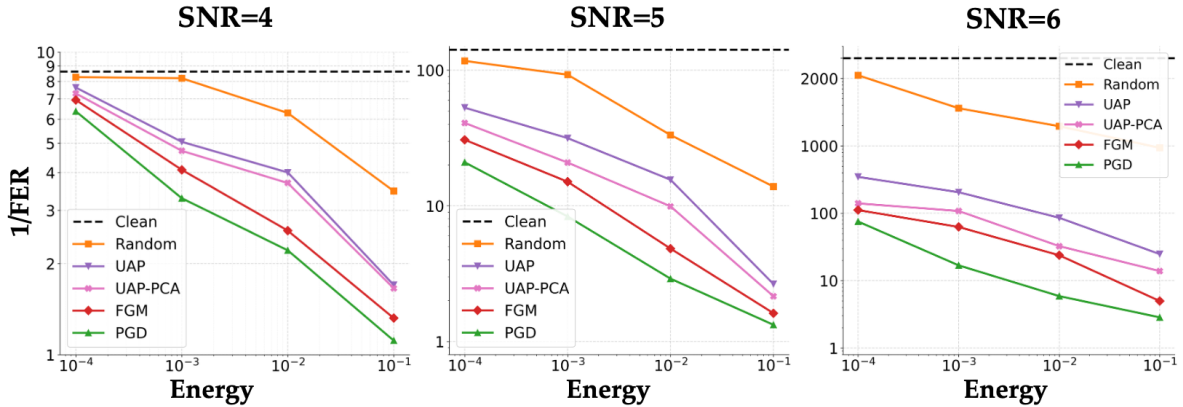


Figure 2: Comparison of **FER-Inverse (1/FER)** under various energy constraints for ECCT on LDPC(121,60).

D.2 Transferability of Adversarial Perturbation

In this section, we present additional results regarding the transferability of adversarial perturbations. Specifically, we generate optimal perturbations using both the universal method (UAP) and the sample-level method (PGD) targeting the ECCT model on LDPC(121,60) (Table 3) and Polar(128,64) (Table 4) codes. We then evaluate these perturbations against various baselines, including AI-based decoders (ECCT, CrossMPT, and the diffusion-based DDECC [42]) and traditional decoders (Min-sum, Sum-product for LDPC and SC (Successive Cancellation) [43], Sum-product for Polar). The results demonstrate that adversarial attacks exhibit strong transferability across AI decoders, whereas traditional decoders remain robust, highlighting the inherent fragility of neural-based decoding architectures.

Table 3: Evaluation of attack transferability measured by **FER-Inverse (1/FER)** across decoders on LDPC(121,60).

Type	Decoder	Attack	4 dB	5 dB	6 dB
AI Decoder	ECCT	Clean	8.6×10^0	1.4×10^2	1.1×10^4
		Random	8.2×10^0	9.3×10^1	3.6×10^3
		UAP	5.1×10^0	3.2×10^1	8.0×10^2
		PGD	3.3×10^0	8.3×10^0	1.7×10^1
AI Decoder	CrossMPT	Clean	2.1×10^1	6.1×10^2	1.7×10^4
		Random	1.9×10^1	2.7×10^2	3.8×10^3
		UAP	1.7×10^1	6.7×10^1	8.8×10^2
		PGD	9.2×10^0	3.2×10^1	5.5×10^1
AI Decoder	DDECC	Clean	1.7×10^1	5.5×10^2	1.4×10^4
		Random	1.6×10^1	2.4×10^2	3.2×10^3
		UAP	1.4×10^1	6.5×10^1	9.5×10^2
		PGD	9.5×10^0	4.3×10^1	7.3×10^1
Traditional Decoder	Min-sum	Clean	5.4×10^0	5.1×10^1	2.0×10^3
		Random	5.4×10^0	5.1×10^1	1.9×10^3
		UAP	5.3×10^0	5.0×10^1	1.7×10^3
		PGD	5.0×10^0	4.3×10^1	1.3×10^3
Traditional Decoder	Sum-product	Clean	1.6×10^1	4.9×10^2	1.5×10^4
		Random	1.6×10^1	4.8×10^2	1.4×10^4
		UAP	1.5×10^1	4.1×10^2	1.1×10^4
		PGD	1.3×10^1	3.3×10^2	1.0×10^4

Table 4: Evaluation of attack transferability measured by **FER-Inverse (1/FER)** across decoders on Polar(128,64).

Type	Decoder	Attack	4 dB	5 dB	6 dB
ECCT	AI Decoder	Clean	8.5×10^0	7.4×10^1	1.4×10^3
		Random	8.1×10^0	5.9×10^1	6.1×10^2
		UAP	5.4×10^0	3.4×10^1	9.8×10^1
		PGD	3.0×10^0	5.4×10^0	8.3×10^0
CrossMPT	AI Decoder	Clean	2.5×10^1	2.4×10^2	1.0×10^4
		Random	2.2×10^1	1.8×10^2	5.8×10^3
		UAP	1.9×10^1	8.4×10^1	9.2×10^2
		PGD	5.1×10^0	9.1×10^0	4.9×10^1
DDECC	AI Decoder	Clean	5.2×10^1	7.4×10^3	9.7×10^5
		Random	4.9×10^1	6.5×10^3	7.1×10^5
		UAP	2.7×10^1	2.1×10^3	3.5×10^4
		PGD	9.7×10^0	7.5×10^2	2.2×10^2
SC	Traditional Decoder	Clean	4.2×10^0	3.8×10^1	4.5×10^2
		Random	4.1×10^0	3.7×10^1	4.2×10^2
		UAP	3.8×10^0	3.4×10^1	3.7×10^2
		PGD	3.5×10^0	3.2×10^1	3.5×10^2
Sum-product	Traditional Decoder	Clean	5.6×10^0	5.9×10^1	6.8×10^2
		Random	5.4×10^0	5.7×10^1	6.5×10^2
		UAP	5.1×10^0	5.2×10^1	6.0×10^2
		PGD	4.9×10^0	5.0×10^1	5.6×10^2